JOURNAL OF PROPULSION AND POWER
Vol. 26, No. 3, May–June 2010

# Optimal Design of Hybrid Rocket Motors for Launchers Upper Stages

Lorenzo Casalino* and Dario Pastrone†
*Politecnico di Torino, 10129 Turin, Italy*

DOI: 10.2514/1.41856

**A hybrid rocket is considered as the third stage of a three-stage launcher. The design of the hybrid rocket motor and the trajectory are simultaneously optimized by means of a nested direct/indirect procedure. Direct optimization of the parameters that affect the motor design is coupled with indirect trajectory optimization to maximize the launcher payload for assigned characteristics of the first and second solid-propellant stages and final orbit. A mission profile based on the Vega launcher is considered. The feed system exploits a pressurizing gas, namely, helium, with hydrogen peroxide as the oxidizer and polyethylene as the fuel. The simplest blowdown design is compared with a more complex pressurizing system, which has an additional gas tank that allows for a phase with constant oxidizer tank pressure. The optimization provides the optimal values of the main engine design parameters (pressurizing gas mass, nozzle expansion ratio, and initial values of tank pressure, mixture ratio, and thrust), the corresponding grain and engine geometry, and the control law (thrust direction during the ascent trajectory and engine switching times). Results show that a hybrid rocket may be a viable option for small launchers.**



## Nomenclature

| | | |
|---|---|---|
| $A_b$ | = | burning surface area, $m^2$ |
| $A_p$ | = | port area, $m^2$ |
| $A_{th}$ | = | nozzle throat area, $m^2$ |
| $a$ | = | regression constant, $m^{1+2n} \cdot kg^{-n} \cdot s^{n-1}$ |
| $C_{Dj}$ | = | $j$th stage drag coefficient |
| $C_F$ | = | thrust coefficient |
| $c^*$ | = | characteristic velocity, m/s |
| $\boldsymbol{D}$ | = | drag vector, N |
| $\boldsymbol{F}$ | = | thrust vector, N |
| $F$ | = | thrust magnitude, N |
| $\boldsymbol{g}$ | = | gravity acceleration, $m/s^2$ |
| $h$ | = | initial port dimension, m |
| $I_{sp}$ | = | specific impulse, s |
| $J$ | = | throat area to initial port area ratio |
| $L$ | = | overall length, m |
| $L_b$ | = | grain length, m |
| $M$ | = | rocket mass, kg |
| $m$ | = | mass, kg |
| $N$ | = | number of ports |
| $n$ | = | mass-flux exponent |
| $P$ | = | burning perimeter, m |
| $p$ | = | pressure, bar |
| $p_{din}$ | = | dynamic pressure, kPa |
| $R$ | = | radius, m |
| $R_g$ | = | grain outer radius, m |
| $R_{th}$ | = | throat radius, m |
| $\boldsymbol{r}$ | = | position vector, m |
| $S_j$ | = | $j$th stage reference area, $m^2$ |
| $t$ | = | time, s |
| $V$ | = | volume, $m^3$ |
| $\boldsymbol{v}$ | = | velocity vector, m/s |
| $w$ | = | web thickness, m |
| $x$ | = | port angular fraction |
| $y$ | = | burned distance, m |
| $Z$ | = | hydraulic resistance, $(kg \cdot m)^{-1}$ |
| $\alpha$ | = | mixture ratio |
| $\beta$ | = | angle, rad |
| $\gamma$ | = | specific heat ratio |
| $\varepsilon$ | = | nozzle area ratio |
| $\rho$ | = | density, $kg/m^3$ |
| $\phi$ | = | free molecular thermal flux, $W/m^2$ |

*Subscripts*

| | | |
|---|---|---|
| $a$ | = | auxiliary gas |
| atm | = | atmospheric |
| avg | = | average |
| bd | = | beginning of blowdown phase |
| $c$ | = | combustion chamber at nozzle entrance |
| cc | = | combustion chamber |
| $e$ | = | nozzle exit |
| $F$ | = | fuel |
| $g$ | = | pressurizing gas |
| gt | = | pressurizing gas tank |
| $i$ | = | initial value |
| $n$ | = | nozzle |
| $O$ | = | oxidizer |
| $p$ | = | overall propellant (oxidizer + fuel) |
| rc | = | rocket casing |
| rel | = | relative |
| res | = | residual |
| $s$ | = | hybrid rocket structural mass |
| $t$ | = | oxidizer tank |
| th | = | throat |
| $u$ | = | payload |
| 1 | = | combustion chamber at the head end |

*Superscript*

| | | |
|---|---|---|
| $\dot{}$ | = | time derivative |

Presented as Paper 4541 at the 44th AIAA/ASME/SAE/ASEE Joint Propulsion Conference & Exhibit, Hartford, CT, 21–23 July 2008; received 28 October 2008; revision received 2 December 2009; accepted for publication 11 January 2010. 

*Associate Professor, Dipartimento di Energetica, Corso Duca degli Abruzzi, 24 Torino. Senior Member AIAA.

†Associate Professor, Dipartimento di Energetica, Corso Duca degli Abruzzi, 24 Torino. Senior Member AIAA.

## I. Introduction

SOLID propellants allow for compact stages, because they have high values of density-specific impulse. This fact makes them suitable for launcher first stages. Moreover, without pumps and valving, solid motors are reliable. Their application as upper stages

suffers from low performance and no capability of shutoff control. The low specific impulse penalizes the final part of ascent, reducing the launcher performance, while the lack of flexibility may determine a large scattering in the orbit insertion parameters.

Liquid rocket engines overcome these problems, having a higher specific impulse than solids and flexible stop and restart capabilities. Liquid oxygen (LOX) is commonly used as the oxidizer, with either liquid hydrogen (LH2) or RP-1 as the fuel. The LOX/LH2 combination presents very high performance, but both propellants are cryogenic. On the other hand, RP-1 reduces problems related to low temperatures, but performance is affected. The use of storable propellants, typically nitrogen tetroxide (NTO) with monomethyl hydrazine (MMH) or unsymmetrical-dimethyl hydrazine (UDMH), provide performance close to that of the LOX/RP-1 combination. Anyway, these propellants have limited applications due to heavy engine and tanks, hazards, environmental reasons, and costs. Solid rocket motors are now commonly employed in small launchers (Minotaur, Pegasus, Taurus, Start-1, Vega). A liquid-propellant upper stage is sometimes used, because of its shutdown–restart capability, which guarantees a greater precision in the orbit injection.

The performance of a hybrid rocket motor (HRM) is similar to that of storable liquid propellants. Because the oxidizer is stored apart from the fuel, HRMs can be shut off and restarted like liquid rocket engines and can be throttled within a wide thrust range. They are safe, reliable, and relatively low cost and have a reduced environmental impact. Moreover, special safety steps needed for chemicals such as NTO, MMH, and UDMH are eliminated, and operation costs fall as a result. Hybrid-propellant rockets have already been proposed to replace solid-propellant rockets, with particular emphasis on booster stages [1–5]; moreover, a hybrid motor was used for a manned suborbital flight to a 100 km altitude [6] and will be probably employed for commercial space flights [7]. However, the features of hybrid propellants also make HRMs suitable for replacing solid rocket motors and storable liquid rocket engines used in launchers' upper stages [8,9]. Their use as the third and final stage of a low-cost launcher is particularly attractive and is investigated here.

Because of the peculiar combustion process of hybrid motors, the determination of the strategy for obtaining high specific impulse is more complex than in solid and liquid rockets. In solid rockets the mixture ratio is assigned and the chamber pressure is dictated by the grain and nozzle geometry, whereas in bipropellant liquid engines both the chamber pressure and mixture ratio can be controlled to set the best propellant consumption for the required thrust level. Hybrid rocket motors cannot be operated in the same manner due to the "one-lever" feature: the fuel flow coming from the grain is a nonlinear function of the oxidizer flow and the mixture ratio cannot be chosen independently when the thrust level is assigned, unless a portion of oxidizer mass flow bypasses the grain ports. Moreover, it should be pointed out that the optimization of the motor design and operations is strictly related to the type of mission considered. Thrust has a major influence, because it affects both the motor design and the trajectory performance; a compromise must be sought, as greater thrusts reduce the gravitational losses while increasing structural mass. Therefore, the design optimization should include trajectory analysis and, possibly, its optimization.

The aim of the present paper is to evaluate the performance that can be obtained by using HRMs to upgrade existing/in-development low-cost launchers that employ solid rocket motors and/or storable liquid propellants for powering upper stages. In particular, the use of a hybrid motor as the third and final stage of a launcher is proposed. This analysis is pursued via a multidisciplinary optimization approach that couples the optimization of the propulsion system and trajectory. The design parameters are optimized by means of a direct method, in conjunction with an indirect procedure to optimize the trajectory. The performance index to be maximized is the payload inserted into a reference orbit. The optimal values for the propulsion system parameters are sought, while holding the characteristics of the lower stages of the launcher unchanged.

Reference is made to the Vega launcher [10], which has three solid-propellant stages and a fourth liquid-propellant stage and which is first ignited to complete the boost phase and then performs a second burn for the injection into the final orbit. Here, a hybrid motor replaces the third and fourth stages and is designed to perform the injection into the final orbit by means of two burns. Hydrogen-peroxide (HP)/polyethylene (PE) is the propellant combination. A gas-pressure feed system is adopted because of its simplicity and lower cost compared to pump-fed engines. To assess the benefit provided by the oxidizer mass flow control while facing complexity, the blowdown feed system option is first considered and then compared to a partially regulated pressure system.

## II. Grain Geometry and Ballistic Model

A multiport grain geometry is adopted, while considering a uniform regression rate along the port axis. A simple circular-section grain [11] with either 6 or 8 ports is adopted; different grain geometries could provide improved performance and packaging efficiency [12] but are not considered here. The grain geometry, described in Fig. 1, is defined by the number of ports $N$, the web thickness $w$, and the grain outer radius $R_g$. One has the following:

$$x = (N/\pi)\sin^{-1}[w/(R_g - w)] \tag{1}$$

$$h = \sqrt{(R_g - w)^2 - w^2} - w\tan(\pi/2 - \pi/N) \tag{2}$$

$$\beta = \pi/2 + x\pi/N \tag{3}$$

The initial port area is then easily determined:

$$(A_p)_i = 2N[(R_g - w)^2(1 - x)\pi/(2N) - hw/2)] \tag{4}$$

For a given burning distance $y$ ($0 \le y \le w$), one easily computes the burning perimeter

$$P = 2N[(R_g - w + y)(1 - x)\pi/N + \beta y + h + (\pi/2 - \pi/N)y] \tag{5}$$

and the port area

$$A_p = (A_p)_i + 2N\{[(R_g - w + y)^2 - (R_g - w)^2](1 - x)\pi/(2N) + \beta y^2/2 + hy + (\pi/2 - \pi/N)y^2/2\} \tag{6}$$

The regression rate is determined by the oxidizer mass flux and grain geometry:

$$\dot{y} = a(\dot{m}_O/A_p)^n \tag{7}$$

with $a = 7 \times 10^{-6}$ and $n = 0.8$, when SI units are used [13,14]. The mass fluxes obtained in this article always fall in the validity range (20–1000 kg/s/m$^2$) of this curve fit. No pyrolysis of the lateral ends is considered. Pressure losses inside the combustion chamber are taken into account by relating the chamber head-end pressure $p_1$ to the chamber nozzle-stagnation pressure $p_c$. An approximate relation, similar to that proposed by Barrere et al. [15] for solid-propellant side-burning grains, is used:

$$p_1 = [1 + 0.2(A_{\text{th}}/A_p)^2]p_c \tag{8}$$

The pressure loss is typically between 2 and 5%, consistent with HRM operation (see, for instance, [2]). The hydraulic resistance $Z$ in the oxidizer flowpath from the tank to the combustion chamber determines the oxidizer flow rate. Under the assumption of incompressible turbulent flow,

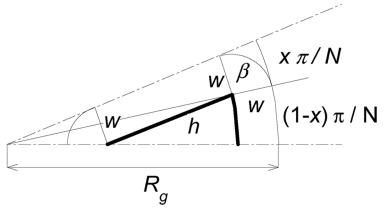


**Fig. 1 Grain geometry.**

$$\dot{m}_O = \sqrt{(p_t - p_1)/Z} \tag{9}$$

The value of $Z$ is assumed to be constant during motor operation. The fuel mass flow is obtained as

$$\dot{m}_F = \rho_F \dot{y} A_b = \rho_F \dot{y} L_b P \tag{10}$$

and the mixture ratio is

$$\alpha = (\dot{m}_O/\dot{m}_F) \propto \dot{m}_O^{1-n} A_p^n / A_b \tag{11}$$

An isentropic expansion in the nozzle is assumed, and the chamber nozzle-stagnation pressure $p_c$ is determined by

$$p_c = \frac{(\dot{m}_O + \dot{m}_F) c^*}{A_{\text{th}}} \tag{12}$$

The performance of the propellant combination is evaluated [16] as a function of the mixture ratio $\alpha$, assuming $p_c = 10$ bar. Even though the actual pressure in the combustion chamber can span over a wide range during motor operations, the error is small for the chamber pressures and mixture ratios considered in this paper. Frozen equilibrium expansion is assumed; the exhaust gas maintains throughout the nozzle the composition that it has in the combustion chamber. This conservative assumption of frozen equilibrium expansion is adopted to account for the low combustion efficiency of HRMs; in addition a 0.96 $c^*$ efficiency [17] is introduced. Third-degree polynomial curves fitting the characteristic velocity and specific heat ratio are embedded in the code to compute the proper values as the mixture ratio changes during motor operations.

## III. Motor Design and Operation

According to the chosen ballistic model, the design of the HRM is defined by the following: 1) initial thrust level $F_i$, 2) initial mixture ratio $\alpha_i$, 3) nozzle expansion ratio $\varepsilon$, 4) initial value of tank pressure $(p_t)_i$, 5) initial value of chamber pressure $(p_c)_i$, and 6) ratio $J$ of the throat area to the initial port area.

The initial chamber pressure is assigned by imposing $(p_c)_i = 0.4(p_t)_i$; actually, the ratio $p_t/p_c$ varies during operation, but the assumed initial ratio is usually sufficient to guarantee $p_t/p_c > 1.5$ and to avoid coupling between the hybrid motor and the oxidizer feed system. The initial port area to throat area ratio $J$ influences both motor geometry (and weight) and operation (namely, the mixture-ratio shift and the corresponding change of specific impulse); preliminary results showed that the optimization would require quite large values of $J$; in the present article, its value is fixed at $J = 0.5$ to avoid excessive pressure losses and nonuniform grain regression, typically related to larger values of $J$. Additional parameters are to be given, depending on the feed system. Two different options, namely, blowdown and partially regulated, are considered here for a pressurizing feed system that uses compressed gas.

When the blowdown feed system is adopted, only the mass of pressurizing gas, which is initially stored in the oxidizer tank, is required. The addition of $m_g$ to the set of free design parameters would lead to very small values of the regression rate, in particular, at the end of operation. Grain cooking occurs when the regression rates becomes lower than a critical value, typically 0.2 mm/s; to avoid grain cooking, the condition that fixes the final value of the regression rate at 0.2 mm/s is added to the boundary conditions of the ascent trajectory, implicitly determining $m_g$. For practical reasons, the mass of pressurizing gas is actually replaced by $(V_g)_i$, that is, the volume of the oxidizer tank that is initially filled by the pressurizing gas (initial ullage volume), as an additional unknown of the trajectory indirect optimization.

A partially regulated feed system is also considered: a phase with constant tank pressure, maintained by means of helium flowing from an auxiliary tank, is introduced, followed by a blowdown phase. In addition to $(V_g)_i$, the initial pressure in the gas tank and the length of the constant-pressure phase must be known to determine the tank pressure history. The initial ullage volume is assumed to be 3% of the overall oxidizer volume $(m_O)_f/\rho_O$, to have a stable regulator response when the outflow starts [18]. The total oxidizer mass $(m_O)_f$ and, consequently, $(V_g)_i$ can only be obtained at burnout, and a tentative value, which becomes an additional unknown of the ascent trajectory, is necessary to start the integration; the tentative value for $(m_O)_f$ is corrected by the trajectory indirect optimization procedure to match the value obtained at burnout by integrating Eq. (9). The initial pressure in the gas tank is fixed at $p_a = 200$ bar, even though improved performance could be obtained by increasing its value. The time length of the regulated phase is conveniently defined by means of the oxidizer mass, which has been exhausted at the start of the blowdown phase $(m_O)_{\text{bd}}$; $(m_O)_{\text{bd}}$ becomes an additional optimization variable. However, solutions with $\dot{y}_f$ lower than 0.2 mm/s would be obtained with an unconstrained optimization, and the constraint on the final value of the regression rate is again added to the boundary conditions of the ascent trajectory. As a consequence, $(m_O)_{\text{bd}}$ is dropped from the optimization variables and becomes a parameter of the ascent trajectory, which implicitly determines the time length of the phase with constant pressure in the oxidizer tank and the gas mass $m_g$.

When the tank pressure is kept constant, $p_t = (p_t)_i$, whereas $p_t$ is calculated assuming an isentropic expansion of the pressurizing gas in the tank during the subsequent blowdown phase:

$$p_t = (p_t)_i \left[\frac{(V_g)_{\text{bd}}}{V_g}\right]^{\gamma_g} \tag{13}$$

where $(V_g)_{\text{bd}}$ is the gas volume in the propellant tank at the start of the blowdown phase and $V_g$ its value at time $t$. One has $V_g = (V_g)_i + m_O/\rho_O$ and either $(V_g)_{\text{bd}} = (V_g)_i$ (when the simpler blowdown pressurization is chosen) or $(V_g)_{\text{bd}} = (V_g)_i + (m_O)_{\text{bd}}/\rho_O$ (for the regulated feed system). The design parameters are optimized as shown in Sec. IV.

Given the set of design parameters, the motor geometry is first determined. The relevant properties of the combustion gases can be computed, owing to the fact that the initial values of $c^*$ and $\gamma$ can be calculated from $\alpha_i$ via the aforementioned curve fittings. The thrust coefficient $C_F$ can then be evaluated by assuming an isentropic one-dimensional expansion with constant $\gamma$, provided the ambient pressure is known. With a 0.98 thrust correction factor introduced to modify the vacuum thrust coefficient, one has

$$C_F = 0.98\left\{\sqrt{\frac{2\gamma^2}{\gamma-1}\left(\frac{2}{\gamma+1}\right)^{\frac{\gamma+1}{\gamma-1}}\left[1-\left(\frac{p_e}{p_c}\right)^{\frac{\gamma-1}{\gamma}}\right]} + \varepsilon\frac{p_e}{p_c}\right\} - \varepsilon\frac{p_{\text{atm}}}{p_c} \tag{14}$$

where the term related to the atmospheric pressure is always small, as the third stage always flies at high altitude. The mass flow rates at rocket ignition (i.e., at $t = 0$) are found from the initial thrust $F_i$:

$$(\dot{m}_p)_i = (1+\alpha_i)(\dot{m}_F)_i = \frac{1+\alpha_i}{\alpha_i}(\dot{m}_O)_i = \frac{F_i}{c_i^*(C_F)_i} \tag{15}$$

The throat and initial port areas $A_{\text{th}}$ and $(A_p)_i$ are then determined:

$$A_{\text{th}} = \frac{(\dot{m}_p)_i}{(p_c)_i c_i^*}; \qquad (A_p)_i = \frac{A_{\text{th}}}{J} \tag{16}$$

The nozzle throat area $A_{\text{th}}$ is considered to be constant during operation. One also finds

$$(A_b)_i = \frac{(A_p)_i^n}{a\rho_F}\frac{(\dot{m}_F)_i}{(\dot{m}_O)_i^n} \tag{17}$$

The grain geometry can then be derived once a tentative value is assumed for $R_g$. Equations (1–4) are numerically solved for $x$, $\beta$, $h$, and $w$ given the required initial port area. Equation (5) at ignition ($y = 0$) gives the initial perimeter $P_i$ to compute the grain length $L_b = (A_b)_i/P_i$. Equation (7) is integrated up to burnout during the optimization of the ascent trajectory. The ascent optimization procedure corrects the tentative value for $R_g$ to match the necessary condition $y_f = w$ at burnout.

The head-end pressure is computed with Eq. (8) and, knowing the initial tank pressure, the hydraulic resistance $Z$ can also be determined by applying Eq. (9) at $t = 0$. The motor geometry is completely defined and, once the initial ullage volume in the propellant tank has been assumed and the pressurization system has been specified, the motor performance can be evaluated during operation.

The tank pressure rules motor operation; either $p_t = (p_t)_i$ or $p_t$ is provided by Eq. (13). Numerical integration of Eqs. (7), (9), and (10) allows the evaluation of the fuel grain geometry, the exhausted masses of oxidizer and fuel, and their mass flow rates. At each instant $t$, once the tank pressure $p_t$ and the motor geometry are known, the regression rate, the propellant flow rates (and their ratio $\alpha$), $c^*$, $p_c$, and $p_1$ are computed by numerically solving Eqs. (7–12) while the curve fit for $c^*$ as a function of $\alpha$ is used. Then, the thrust level $F = p_c A_{\text{th}} C_F$ is determined by evaluating $C_F$ at the actual altitude via Eq. (14), to integrate the trajectory equations. At burnout the overall propellant mass is finally evaluated, and an estimation of the structural masses can be obtained.



## IV. Optimization

The optimization procedure aims at finding the motor design parameters and the corresponding trajectory that maximize the mission performance index, which is, in this article, the payload inserted into a prescribed orbit. As the number of motor design parameters is low (four, in this case), their optimization is easily carried out by a direct method. Also, the relations, which determine the motor behavior, cannot be written explicitly and indirect methods cannot be used. On the other hand, the trajectory optimization is characterized by continuous controls (namely, the thrust direction), which would either require a discretization by means of a large number of parameters or the use of indirect methods. A mixed optimization procedure [19] is adopted here. An indirect method [20] optimizes the trajectory for each choice of the motor parameters. These are instead optimized by means of a direct procedure [21]. Both methods have been developed at the Politecnico di Torino.

Tentative values are initially assumed for the design parameters, that is, $F_i$, $\alpha_i$, $\varepsilon$, and $(p_t)_i$. For each set of parameters, the fast and accurate indirect procedure provides the optimal trajectory and the corresponding performance index; a few seconds are required when a 2 GHz PC is used. The design parameters are then varied by small quantities to numerically evaluate the derivatives of the performance index with respect to the design parameters. To find the maximum performance index, a procedure based on Newton's method is used to determine the set of design parameters that simultaneously nullify the index partial derivatives. Only a few minutes are sufficient to obtain the optimal design and the corresponding trajectory.

A point mass rocket is considered for the trajectory optimization. The state equations provide the derivative of position $\boldsymbol{r}$ (radius, latitude, and longitude), velocity $\boldsymbol{v}$ (radial, eastward, and northward components), and rocket mass $M$. The equations of motion are written in nondimensional form to improve the integration's numerical accuracy. In a vectorial form, one has

$$\frac{\mathrm{d}\boldsymbol{r}}{\mathrm{d}t} = \boldsymbol{v} \qquad \frac{\mathrm{d}\boldsymbol{v}}{\mathrm{d}t} = \boldsymbol{g} + \frac{\boldsymbol{F} - \boldsymbol{D}}{m} \qquad \frac{\mathrm{d}M}{\mathrm{d}t} = -\frac{|\boldsymbol{F}|}{c^* C_F} \tag{18}$$

An inverse-square gravity field is assumed and $D = (1/2)\rho_{\text{atm}} C_{Dj} S_j v_{\text{rel}}^2$ is the aerodynamic drag magnitude; each subrocket has an assigned reference area $S_j$, and the drag coefficient $C_{Dj}$ is a known function of the Mach number; the relative velocity is evaluated taking the Earth's rotation into account. The thrust is written as a function of the vacuum thrust: $F = F_{\text{vac}} - \epsilon A_{\text{th}} p_{\text{atm}}$. Numerical fits of the U.S. Standard Atmosphere are used to determine pressure, density, and temperature as functions of the altitude for the determination of drag and thrust.

The performance of a rocket with characteristics similar to those of the European small launcher Vega [10] are evaluated and used as a reference case. Gross and propellant masses and thrust profiles of the first three solid-propellant stages and the fourth liquid-propellant stage are assigned; the payload is maximized for a 700 km circular polar orbit. The same initial mass and trajectory constraints of the reference case are assumed for the three-stage launchers with a hybrid upper stage; also, the characteristics of the first two solid-propellant stages are unchanged. Given the initial mass, the gross masses of the first two stages, and the fairing mass, the remaining mass budget is split between hybrid-stage mass and payload; for assigned characteristics of the hybrid rocket, the trajectory is optimized to maximize the final mass and the payload is obtained by subtracting the dry mass of the hybrid rocket (combustion chamber, nozzle, tanks, case; pressurizing gas and propellant residual are also included in the dry mass).

The trajectory is split into phases. The first stage burn is divided into 1) vertical ascent, 2) kick phase, and 3) zero-lift gravity-turn ascent; then the first stage is jettisoned, and a 4) coast phase follows. The second stage burn is a single 5) zero-lift gravity-turn phase followed by the stage jettisoning, and a 6) coast arc. The third stage performs two burns with optimal thrust direction; during the first burn the fairing is jettisoned and the following phases are introduced: 7) first burn with fairing (either blowdown or with constant tank pressure, depending on the adopted pressurizing system), 8) first burn without fairing (constant tank pressure), 9) first burn without fairing (blowdown), 10) coast arc, and 11) second burn (blowdown). When a blowdown pressurization feed system is adopted, the corresponding law is adopted during phase 7 and the length of phase 8 is nullified. The time length of phases 1, 2, 3, 4, 5, 6, and 7 are assigned. The time length of the remaining phases is determined during the trajectory optimization. The vacuum thrust magnitude and the propellant flow rate are assigned functions of time for the solid-propellant rockets, whereas they are provided by the HRM design optimization for the third stage. The thrust direction is vertical during phase 1, parallel to the relative velocity in phases 3 and 5, and free and optimized during phases 2, 7, 8, 9, and 11.

Boundary conditions define the mission to be performed: the initial mass (137,276 kg), position, and velocity are assigned (launch from Kourou is here assumed). The masses of the exhausted stages and fairing are also given. The free molecular heat flux $\phi = (1/2)\rho_{\text{atm}} v_{\text{rel}}^3$ is fixed at 0.1 BTU/ft$^2$/s $= 1135$ W/m$^2$ at the end of phases 7 (i.e., when the fairing is jettisoned) and 9 (first shutdown of the third stage); also, horizontal flight is imposed at the latter point, to prevent the rocket from reentering the lower layers of the atmosphere, where the heat flux would become larger. The final orbit is specified by assigning altitude (700 km), eccentricity (0, i.e., circular orbit), and inclination (90 deg, i.e., polar orbit); the longitude of the ascending node is left free.

The theory of optimal control is applied to optimize the trajectory, given the characteristics of the hybrid-propellant third stage. The details of the indirect optimization procedure can be found in [19,22] and are only summarized here. An adjoint variable is associated to each equation; the theory of optimal control provides the Euler–Lagrange equations for the adjoint variables, the algebraic equations that determine the control variables (i.e., the thrust direction), and the boundary conditions for optimality, which also implicitly define the hybrid motor switching times. The multipoint boundary value problem, which arises from the application of the theory of optimal control, is solved by a procedure [23] based on Newton's method. Tentative values are initially chosen for the problem unknowns and progressively modified to fulfill the boundary conditions. The initial ullage volume $(V_g)_i$ (blowdown case), the oxidizer mass at the start of blowdown $(m_O)_{\text{bd}}$ and its final value $(m_O)_f$ (regulated case), and the grain outer radius $R_g$ (both cases) are additional unknowns of the ascent optimization.

## V. Numerical Results

The optimization procedure, which was described in the previous section, is now applied to the design of a hybrid-propellant third stage with the aim of maximizing the payload delivered into a 700 km polar orbit. For the sake of comparison, the trajectory and performance of a launcher with three solid-propellant stages and a liquid-propellant fourth stage, with characteristics similar to those of the Vega launcher

[10], have been computed and are used as a baseline. The payload of the reference launcher is about 1400 kg, consistent with the performance of Vega. The same constraints on the trajectory are assumed for the launcher with a hybrid-propellant third stage.

The indirect trajectory optimization maximizes the final mass (initial mass minus exhausted propellant) given the engine geometry. The payload is then evaluated by subtracting the mass of the propulsion system, that is, the masses of the combustion chamber, nozzle, tanks, rocket casing, and propellant sliver, from the final mass (feed systems masses, e.g., valves and plumbings, are neglected); these are estimated by means of suitable assumptions and approximations. The combustion chamber has a 6 mm insulating liner (with a density equal to that of the solid fuel) and an aluminum alloy cylindrical wall. The diameter of the aluminum cylindrical oxidizer tank is fixed at 1.9 m, matching the diameter of Vega's third stage. A spherical aluminum tank is used for the pressurizing gas when the partially regulated feed system is adopted. The minimum pressure drop between the gas and oxidizer tanks is conservatively fixed at 10 bar; the required gas mass and gas tank volume can be obtained from the pressure and gas volume in the oxidizer tank at the start of the blowdown phase, which are known from the trajectory integration. The wall thicknesses of the oxidizer tank, gas tank, and combustion chamber are determined to withstand internal pressure, assuming a 1.25 safety factor. The HRM is encapsulated by a 1-mm-thick cylindrical aluminum casing. A 45 deg convergent and a 20 deg divergent nozzle with a phenolic silica ablative layer is considered. A uniform thickness is assumed and is evaluated according to [24] using average values of the transport properties and an estimation of the heat flux at ignition; these assumptions are conservative and the nozzle mass is therefore overestimated; a more detailed analysis is left for future work. The nozzle structural mass is small compared to the ablative layer mass and is thus neglected. Grains with either six or eight ports are considered.

The optimization procedure determines the nozzle expansion area ratio and the initial values of thrust, mixture ratio, and tank pressure. Their values are dictated by the opposite requirements of keeping the system dry mass low, while assuring a large specific impulse and low velocity losses during the ascent to orbit to increase the final mass. The mixture ratio influences the required propellant mass and the motor dry mass; the propellant mass is minimum when the value corresponding to the maximum specific impulse (about 6.7, in the present case) is adopted, but larger values of mixture ratio reduce the system dry mass; the choice of $\alpha_i$ must also consider that $\alpha$ varies during operation. A large nozzle expansion area ratio improves the specific impulse (the third stage always flies in vacuumlike conditions) but increases the nozzle mass.

The choice of initial thrust magnitude, initial tank pressure, and mass of pressurizing gas is influenced by the presence of the constraint on the final value of the regression rate and also depends on the grain geometry. A large thrust value is usually preferable to reduce gravitational losses and increase the regression rate, but it implies a larger dry mass. Large values of both initial tank pressure and mass of pressurizing gas allow for larger regression rates but increase the structural mass. As stated previously, $F_i$ and $(p_t)_i$ are optimized, whereas, in the present analysis, the mass of pressurizing gas is dropped from the optimization and determined to fulfill the regression rate constraint for each combination of the motor optimization variables. Results are summarized in Tables 1 and 2. The "motor-only" propellant fraction $m_p/(m_p + m_s)$ with $m_s = m_{\text{res}} + m_g + m_t + m_{\text{gt}} + m_n + m_{\text{cc}}$ is shown to allow for comparison with existing rockets.

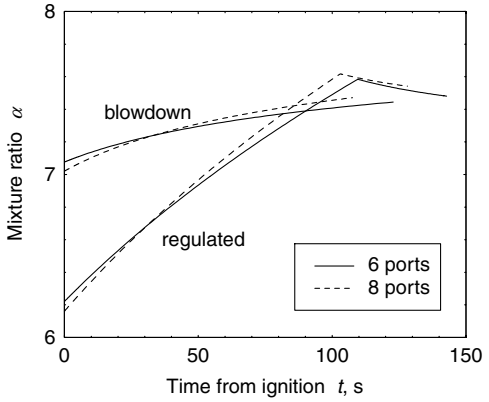


**Fig. 2 Mixture ratio.**

For the selected geometry, a larger number of ports allows for an increase of the burning perimeter and determines a reduction of the grain length, with a small benefit to the system dry mass (the length reduction also improves structural robustness). However, results show that the use of an eight-port grain reduces the performance in terms of payload. In fact, it causes a larger mixture-ratio shifting during engine operation, as shown in Fig. 2, which presents the mixture-ratio histories during the first burn of the HRM. Note that the final burn has a very short duration, 5–6 s, and has a limited influence on the rocket performance; even though the final burn is accounted for during the performance evaluation (neglecting gas warming and the corresponding pressure change during the coast arc), it is not shown in the figures.

The port area grows and causes the mixture ratio increase, offsetting the opposite effects of $\dot{m}_O$ and $A_b$ [see Eq. (11)]. The growth in $A_p$ is more rapid when eight smaller ports are adopted, compared to the six-port case, producing a larger mixture-ratio shifting and also a larger decrease in the regression rate. For this reason, larger values of initial thrust and tank pressure are required to fulfill the constraint on $\dot{y}_f$, causing larger values of maximum acceleration. The larger mixture-ratio shifting reduces the average specific impulse and increases the propellant consumption required to perform the given mission, thus reducing the payload. The eight-port grains are also penalized by the larger sliver.

When the regulated feed system is adopted, the oxidizer flow rate remains almost constant during the phase with constant tank pressure, causing the mixture ratio to increase [see again Eq. (11)] and increasing the propellant consumption. However, because the

**Table 1 HRM optimal design**

| Feed system | $N$ | $F_i$, kN | $\alpha_i$ | $(p_t)_i$, bar | $\epsilon$ | $\alpha_{\text{avg}}$ | $(I_{\text{sp}})_{\text{avg}}$, s | $R_g$, m | $w$, m | $R_{\text{th}}$, m | $L$, m |
|---|---|---|---|---|---|---|---|---|---|---|---|
| Blowdown | 6 | 365.1 | 7.08 | 20.15 | 11.83 | 7.57 | 270 | 0.520 | 0.039 | 0.288 | 12.3 |
| Blowdown | 8 | 414.1 | 7.02 | 19.77 | 11.30 | 7.65 | 271 | 0.558 | 0.034 | 0.310 | 12.0 |
| Regulated | 6 | 209.2 | 6.22 | 13.02 | 11.91 | 7.39 | 272 | 0.508 | 0.042 | 0.271 | 9.8 |
| Regulated | 8 | 230.5 | 6.16 | 12.33 | 11.17 | 7.47 | 271 | 0.546 | 0.037 | 0.293 | 9.4 |

**Table 2 Mass budget**

| Feed system | $N$ | $m_u$, kg | $m_p$, kg | $m_p/m_s$ | $m_{\text{res}}$, kg | $m_g$, kg | $m_t$, kg | $m_{\text{gt}}$, kg | $m_n$, kg | $m_{\text{cc}}$, kg | $m_{\text{rc}}$, kg |
|---|---|---|---|---|---|---|---|---|---|---|---|
| Blowdown | 6 | 1796.1 | 10966.0 | 0.919 | 43.6 | 22.4 | 445.0 | —— | 330.4 | 125.1 | 207.0 |
| Blowdown | 8 | 1774.9 | 10984.0 | 0.918 | 57.2 | 22.3 | 440.3 | —— | 333.8 | 121.5 | 201.5 |
| Regulated | 6 | 1989.4 | 10970.9 | 0.931 | 51.7 | 21.7 | 164.8 | 139.4 | 329.7 | 104.1 | 163.7 |
| Regulated | 8 | 1970.6 | 10989.9 | 0.930 | 67.6 | 21.3 | 156.4 | 136.8 | 335.5 | 100.1 | 157.3 |

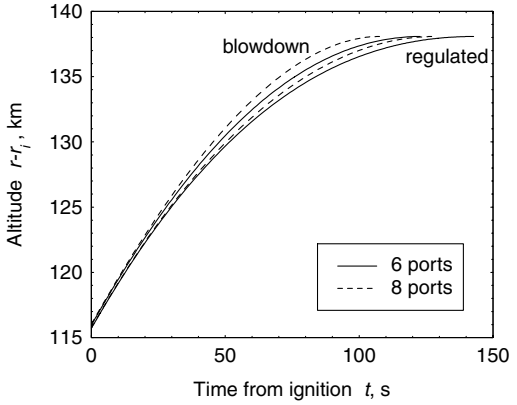


**Fig. 3 Trajectory.**

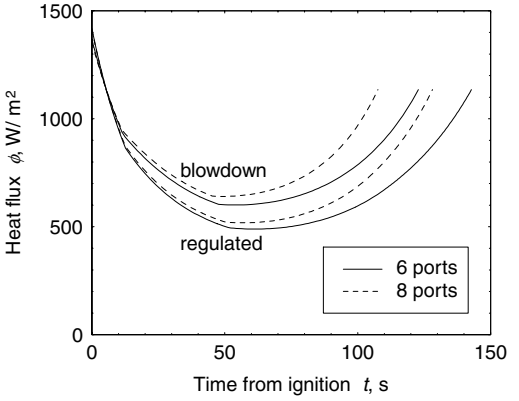


**Fig. 6 Heat flux density.**

pressurizing gas is efficiently stored at large pressure in a small spherical tank, the pressure in the oxidizer tank and its volume can be remarkably reduced; the corresponding decrease of oxidizer tank mass largely offsets the mass penalty of the gas tank and the larger propellant consumption, thus improving the payload while also reducing the rocket length and the maximum value of thrust acceleration. The payload growth is almost 200 kg. The regulated feed system has the additional benefit of reducing the stage length $L$ (the payload length is not included), as the pressurizing gas is stored at the larger pressure $p_a$. The stage length is about 40% larger than that of the third and fourth stages of Vega combined [10] (5.2 m); this situation may be improved by adopting grains with multiple rows of ports [12].

The conditions (height and velocity) at the end of the HRM first burn are almost identical, because they are dictated by the imposed heat flux value and the requirement of leaving the rocket on an ellipse tangent to the final orbit, to perform the orbit insertion with minimum propellant expenditure. However, the trajectories (Fig. 3) exhibit small but significant differences; the blowdown cases require large values of initial thrust, to compensate for the rapid thrust reduction while still fulfilling the constraint on the final regression rate, and exhibit larger average thrust (Fig. 4) and shorter duration. The trajectory is steeper and ignition of the HRM occurs at a slightly higher altitude compared to the regulated cases.

Structural and thermal loads during the first burn of the HRM are shown in Figs. 5 and 6. The longitudinal thrust acceleration exceeds the 5.5 $g$ limit of the Vega launcher [10]. For the sake of comparison, the optimization has also been performed with a constraint, which imposes the final acceleration at 5.5 $g$, added to the set of constraints of the ascent trajectory; in this case, the initial thrust is dropped form the motor design variables and becomes an additional unknown of indirect ascent optimization. The optimal design is modified to fulfill the additional constraint with minimum penalty in terms of payload; smaller values of initial thrust and mixture ratio (a reduction up to 6 and 13%, respectively) and larger values of tank pressure and mass of pressurizing gas (an increase up to 23 and 19%, respectively) are now optimal. Thrust and acceleration are lower during the whole burn, whereas the constraint on the regression rate is still fulfilled. The specific impulse is improved (reducing the propellant consumption), whereas the propulsion system mass (in particular, the tank mass) is increased. The penalty, in terms of payload, is 14.3 kg for the regulated feed system with an eight-port grain, and 30.1 and 1.5 kg for the blowdown feed system with eight and six ports, respectively. The free molecular heat flux has a similar behavior for the four considered cases; it attains the prescribed limiting value of 0.1 BTU/ft$^2$/s when the fairing is jettisoned and at the end of the first burn, and never exceeds this limit after the fairing is jettisoned, as it decreases during the following coast arc.

Even though the results obtained here suffer from simplifications, they clearly show that the introduction of a single hybrid rocket as a replacement for the solid third stage and liquid fourth stage can remarkably improve the launcher performance (the margin ranges from about 400 to almost 600 kg, depending on grain geometry and feed system).

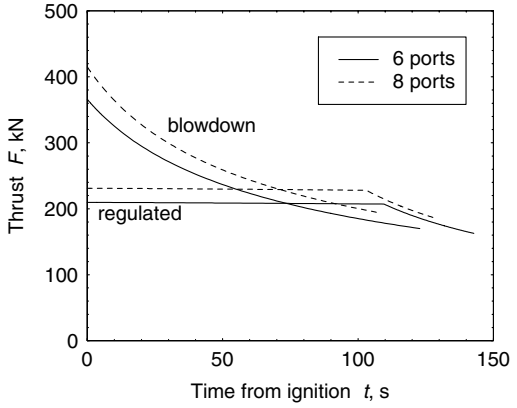


**Fig. 4 Thrust.**

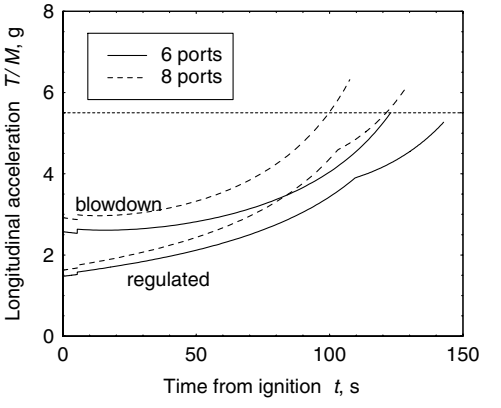


**Fig. 5 Thrust acceleration.**

## VI. Conclusions

An optimization procedure, which couples direct and indirect optimization methods, has been applied to the design optimization of a hybrid rocket to be used as the third stage of a three-stage launcher. The optimization of the parameters that affect the design of the motor is coupled with the trajectory optimization. The coupling is fundamental, as there is a mutual dependence of the mission requirements and engine optimal characteristics. The optimization method is shown to be fast and reliable and provides the motor design and the corresponding trajectory to maximize the payload for given final orbit. A few minutes are sufficient on a standard PC.

The analysis yields results that are similar to those obtained when the mixture-ratio control of liquid rocket engines is analyzed for ascent trajectories: the optimum solutions require mean mixture ratios that are larger than the value that maximizes the specific

impulse to reduce the structural mass. The benefit of the partial regulation of the tank pressure is mainly due to the reduction of the oxidizer tank mass, caused by the reduced tank pressure.

Even though an exact comparison is not possible, the results show that a hybrid third stage can significantly improve the performance compared, for instance, to the use of the combination of a solid-propellant stage with a liquid-propellant upper stage for orbit insertion, while also not increasing (or possibly reducing) the system's simplicity and reliability. The average specific impulse of the HRM, which is found by the optimization procedure to maximize the payload, is slightly lower than that of solid rocket motors used on Vega, and the motor has a comparable (blowdown case) or slightly larger (regulated case) propellant mass fraction [10]; the payload improvement is mainly related to the fact that the liquid-propellant stage (which exhibits a small propellant fraction because it only provides a small velocity increment) is not required, as the HRM synergistically performs the tasks of the third and fourth stages. Other propellant combinations, in particular liquid oxygen and hydroxyl-terminated polybutadiene, and grain geometries (quad port design grains or grains with multiple rows of ports) could be considered to further improve performance and packaging efficiency. Many issues, such as the rocket reignition in a vacuum and the behavior of multiport grains, require further analysis.

## Acknowledgment

The authors thank Guido Colasurdo of the University of Rome "La Sapienza" for his support in the determination of the reference ascent trajectory of the solid/liquid-propellant launcher, which has been used as a baseline for the present work.

## References

[1] Ventura, M. C., and Heister, S. D., "Hydrogen Peroxide as an Alternate Oxidizer for a Hybrid Rocket Booster," *Journal of Propulsion and Power*, Vol. 11, No. 3, 1995, pp. 562–565. doi:10.2514/3.23878

[2] Vonderwell, D. J., Murray, I. F., and Heister, S. D., "Optimization of Hybrid-Rocket-Booster Fuel-Grain Design," *Journal of Spacecraft and Rockets*, Vol. 32, No. 6, 1995, pp. 964–969. doi:10.2514/3.26716

[3] Schoonover, P. L., Crossley, W. A., and Heister, S. D., "Application of a Genetic Algorithm to the Optimization of Hybrid Rockets," *Journal of Spacecraft and Rockets*, Vol. 37, No. 5, 2000, pp. 622–629. doi:10.2514/2.3610

[4] Sackheim, R., Ryan, R., and Threet, E., "Survey of Advanced Booster Option for Potential Shuttle-Derivative Vehicles," AIAA Paper 2001-3414, 2001.

[5] Kwon, S. T., Park, B. K., Lee, C., and Lee, J., "Optimal Design of Hybrid Motor for the First Stage of Air Launch Vehicle," AIAA Paper 2003-4749, 2003.

[6] Dornheim, M. A., "Reaching 100 km," *Aviation Week and Space Technology*, Vol. 161, No. 6, Aug. 2004, pp. 45–46.

[7] Benson, J., "Safe and Affordable Human Access to LEO," AIAA Paper 2005-6758, Sept. 2005.

[8] Jansen, D. P. F. L., and Kletzkine, P., "Preliminary Design for a 3 kN Hybrid Propellant Engine," *ESA Journal*, Vol. 12, No. 4, 1988, pp. 421–439.

[9] Markopoulos, P., and Abel, T., "Development and Testing of a Peroxide Hybrid Upper Stage Propulsion System," AIAA Paper 2001-3243, July 2001.

[10] Isakowitz, S. J., Hopkins, J. A., and Hopkins, J. A., Jr., *International Reference Guide to Space Launch Systems*, 4th ed., AIAA, Reston, VA, 1994.

[11] Ben-Yakar, A., and Gany, A., "Hybrid Engine Design and Analysis," AIAA Paper 1993-2548, July 1993.

[12] Kearney, D. A., Joiner, K. F., Gnau, M. P., and Casemore, M. A., "Improvements to the Marketability of Hybrid Propulsion Technologies," AIAA Paper 2007-6144, Sept. 2007.

[13] Maisonneuve, Y., Godon, J. C., Lecourt, R., Lengelle, G., and Pillet, N., "Hybrid Propulsion for Small Satellites: Design Logic and Test," *Combustion of Energetic Materials*, Begell House, New York, 2002, pp. 90–100.

[14] Wernimont, E. H., and Heister, S. D., "Combustion Experiments in Hydrogen Peroxide/Polyethylene Hybrid with Catalitic Ignition," *Journal of Propulsion and Power*, Vol. 16, No. 2, 2000, pp. 318–326. doi:10.2514/2.5571

[15] Barrere, M., Jaumotte, A., De Veubeke, B. F., and Vandenkerckhove, J., *Rocket Propulsion*, Elsevier, New York, 1960, pp. 251–256.

[16] Mc Bride, B. J., Reno, M. A., and Gordon, S., "CET93 and CETPC: An Interim Updated Version of the NASA Lewis Computer Program for Calculating Complex Chemical Equilibria With Applications," NASA TM-4557, March 1994.

[17] Sutton, G. P., and Biblarz, O., *Rocket Propulsion Elements*, 7th ed., Wiley, New York, 2001, p. 64.

[18] Brown, C. D., *Spacecraft Propulsion*, AIAA Education Series, AIAA, Reston, VA, 1996, p. 82.

[19] Casalino, L., and Pastrone, D., "Optimal Design and Control of Hybrid Rockets for Access to Space," AIAA Paper 2005-3547, July 2005.

[20] Casalino, L., Colasurdo, G., and Pastrone, D., "Optimal Low-Thrust Escape Trajectories Using Gravity Assist," *Journal of Guidance, Control, and Dynamics*, Vol. 22, No. 5, 1999, pp. 637–642. doi:10.2514/2.4451

[21] Casalino, L., and Pastrone, D., "Oxidizer Control and Optimal Design of Hybrid Rockets for Small Satellites," *Journal of Propulsion and Power*, Vol. 21, No. 2, 2005, pp. 230–238. doi:10.2514/1.6556

[22] Casalino, L., Pastrone, D., and Colasurdo, G., "Integrated Design of Hybrid Rocket Upper Stage and Launcher Trajectory," AIAA Paper 2009-4843, Aug. 2009.

[23] Colasurdo, G., and Pastrone, D., "Indirect Optimization Method for Impulsive Transfer," AIAA Paper 94-3762, Aug. 1994.

[24] Barker, D. H., Kording, J. W., Belnap, R. D., and Hall, A. F., "A Simplified Method of Predicting Char Formation in Ablating Rocket Exit Cones," *Chemical Engineering Progress Symposium Series*, Vol. 61, No. 59, 1965, pp. 108–114.

S. Son
*Associate Editor*